Analysis of thermal emission from the nightside of Venus at 1.51 and 1.55 microns

C.F. Wilson, C.C.C. Tsang, P.G.J. Irwin, F.W. Taylor, B. Bézard, S. Erard, R.W. Carlson, P. Drossart, G. Piccioni, R.C. Holmes

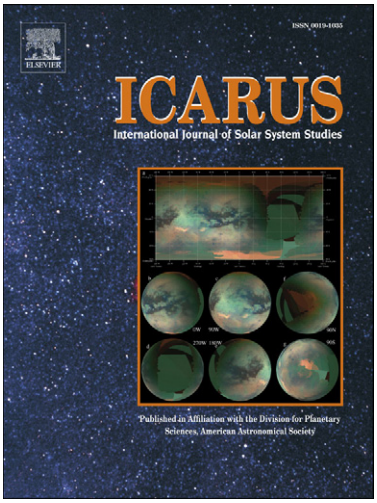

Analysis of thermal emission from the nightside of Venus at 1.51 and 1.55 microns

C.F. Wilson, C.C.C. Tsang, P.G.J. Irwin, F.W. Taylor, B. Bézard, S. Erard, R.W. Carlson, P. Drossart, G. Piccioni, R.C. Holmes

PII: S0019-1035(09)00117-1
DOI: 10.1016/j.icarus.2009.03.010
Reference: YICAR 8961

To appear in: *Icarus*

Received date: 18 August 2008
Revised date: 6 March 2009
Accepted date: 7 March 2009

Please cite this article as: C.F. Wilson, C.C.C. Tsang, P.G.J. Irwin, F.W. Taylor, B. Bézard, S. Erard, R.W. Carlson, P. Drossart, G. Piccioni, R.C. Holmes, Analysis of thermal emission from the nightside of Venus at 1.51 and 1.55 microns, *Icarus* (2009), doi: 10.1016/j.icarus.2009.03.010

Analysis of thermal emission from the nightside of Venus at 1.51 and 1.55 microns

C.F. Wilson
C.C.C. Tsang
P.G.J. Irwin
F.W. Taylor
B. Bézard
S. Erard
R.W. Carlson
P. Drossart
G. Piccioni
R.C. Holmes

Abstract

We present radiative transfer modelling of thermal emission from the nightside of Venus in two 'spectral window' regions at 1.51 and 1.55 μm. The first discovery of these windows, reported by Erard et al. 2009, was achieved using a principal component analysis of data from the VIRTIS instrument on Venus Express. These windows are spectrally narrow, with a full-width at half-maximum of ~20 nm, and less bright than the well-known 1.7 and 2.3 μm spectral windows by two orders of magnitude.

In this note we present the first radiative transfer analysis of these windows. We conclude that the radiation in these windows originates at an altitude of 20-35 km. As is the case for the other infrared window regions, the brightness of the windows is affected primarily by the optical depth of the overlying clouds; in addition, the 1.51 μm radiance shows a very weak sensitivity to water vapour abundance.

Introduction

The atmosphere of Venus is optically thick at most wavelengths below 1 mm, due to its enormous density, one hundred times that of the Earth's atmosphere. However, there are a few narrow spectral regions in the 0.8 – 2.5 μm range at which thermal emission from the deep atmosphere escapes to space. Since the initial discovery of these 'spectral window regions' by Allen & Crawford in 1984, they have been exploited repeatedly by ground-based observations [Crisp et al, 1991; Bézard et al., 1990] and flyby spacecraft [Carlson et al., 1991; Baines et al., 2000], and have been successfully reproduced using radiative transfer modelling [Kamp & Taylor, 1988; Pollack et al., 1993; Tsang et al., 2008]. The brightest window regions are located at 1.74 and 2.3 μm, with more window regions located at 0.85, 0.90, 1.01, 1.10, 1.18, 1.27, and

1.31 μm [Crisp et al., 1991; Lecacheux et al., 1993; Baines et al., 2000]. The relative intensities of the window regions can be seen in the synthetic spectrum shown in Figure 1.

The window regions are located between deep absorption bands of the atmospheric constituents of Venus, primarily CO_2 and water vapour. In the shorter-wavelength windows of 0.85 – 1.01 μm, the atmosphere is optically thin, so virtually all the radiation observed from space originates from the surface. This may make it possible to map the surface temperature and/or emissivity [Baines et al., 2000, Hashimoto et al., 2003]. In the longer wavelength windows of 1.31, 1.74 and 2.3 μm, the radiation originates entirely from the atmosphere (see review in Taylor et al. [1997]). These windows have been used extensively to probe the chemistry of the deep atmosphere, especially the complex window at 2.25 – 2.50 μm which is sensitive to minority constituents CO, OCS, H_2O and SO_2 [e.g. Pollack et al., 1993; Tsang et al., 2008, Marcq et al. 2008].

To the list of IR window regions we can now add 1.51 and 1.55 μm, whose discovery was reported by Erard et al., 2009, however, that paper did not include any radiative transfer modelling. The purpose of the present paper is to confirm that these emission windows are predicted by our radiative transfer models, and to examine what information can be obtained by studying them.

Radiative Transfer Modelling

Fig. 2 (upper left panel) shows a synthetic spectrum of the 1.48 – 1.58 micron region, at a spectral resolution of 1 nm. This is generated using a correlated-k radiative transfer scheme incorporating multi-stream scattering [Irwin et al., 2008]. We have assumed a 4-mode cloud model of sulphuric acid particles as described in Pollack et al., 1993. The temperature profile assumed is that from the Venus International Reference Atmosphere [Seiff et al 1985]. Absorption line parameters for CO_2 are taken from the high-temperature dataset described in Pollack et al., 1993, while absorption lines for H_2O and other gases are taken from the HITRAN2K database [Rothman et al. 2003]. For the far-wing absorption of CO_2

absorption lines, we use a sub-Lorentzian line profile as defined by Tonkov et al., 1996. These modelling assumptions are explained in more detail, and validated, in a paper by Tsang et al, 2008.

The high atmospheric pressure below the clouds of Venus gives rise to significant collision-induced-absorption (CIA) by carbon dioxide molecules, usually modelled as a continuum absorption coefficient α. There have been some laboratory measurements of α but these have all been in the 2.2 – 2.5 μm window; in other windows it has been usual to treat α as a free parameter to be fitted to the data. Typical values of α used by previous authors have ranged from 0 to 3 $\times 10^{-9}$ $cm^{-1}/amagat^2$ at 1.18 – 1.31 μm, and 5 $\times 10^{-9}$ to 8 $\times 10^{-9}$ $cm^{-1}/amagat^2$ for the 1.74 μm window (see discussion in Tsang et al., 2008). We do not *a priori* know what value of α should be used for this new 1.51 μm window; therefore we set this parameter to zero at first. We find an 8 % reduction in the peak radiance if we set the CO_2 CIA coefficient to $\alpha = 8 \times 10^{-9}$ $cm^{-1}/amagat^2$. This sensitivity to the CIA value is relatively small in comparison to that in other window regions; therefore we will continue to assume a value of 0 (no continuum absorption) for our radiative transfer calculations.

To find out at what altitude the radiance originates, we show in the centre panel of Fig. 2 the functional derivative of 1.51 μm radiance with respect to temperature, i.e. the change in radiance which would be observed in each wavelength bin for a change in the temperature at any given level in the model. It can bee seen that this function peaks in an altitude range of 20-35 km, indicating that the thermal emission originates in this region.

The 1.51 and 1.55 μm windows are bounded on both sides by CO_2 absorption bands. Examination of the HITRAN-2k spectral database shows that the strongest absorber in this region after carbon dioxide is water vapour. We therefore also show in figure 2 the functional derivative at 1.51 μm with respect to water abundance, i.e. $dR_{1.51\mu m}/d[H_2O]$. This shows that the radiance at 1.51 μm is sensitive to water vapour abundance at 30-35 km altitude. However, this sensitivity is very weak. A change in water vapour abundance from 30 to 20 ppmv would cause an increase in radiance of only ~1-2 %. Given the low signal-to-noise ratio in this channel, we conclude that these near-IR emission windows are not useful for sensing

chemical abundances in the deep atmosphere. As will be discussed below, however, these window regions could be utilised to constrain cloud properties.

VIRTIS/Venus Express Observations

The Visible and InfraRed Thermal Imaging Spectrometer (VIRTIS) includes an infrared imaging channel which covers a range of 1.05 to 5.14 μm, with a spectral sampling of 9.5 nm. [Piccioni et al, 2008, Drossart et al., 2007]. We have selected VIRTIS observations which used the maximum possible exposure time of 18 seconds. Fig. 3 shows images from two observations: VI0319_00, made on the 5th March 2007, and VI0373_00, made on the 28th April 2007. The first of these observations (shown in the top row) focuses on low-mid latitudes, while the second observation focuses on the polar vortex region. Both observations were made when Venus Express is near its apocentre, high above the Southern pole. The figure shows images at 1.31, 1.51, and 1.74 μm for both observations.

A spatially-dependent correction for scattered sunlight has been made; furthermore, a triangular filter with a FWHM of 3 pixels applied in the horizontal direction in order to reduce an artefact caused by uneven radiometric response of different CCD rows. Finally, we note that the wavelength scale of the VIRTIS-M-IR dataset requires an offset which was found by Bézard et al., 2009 to be typically 5-7 nm at 1.18 μm. For the observations presented in this paper we have established (using radiative transfer modelling of 1.18 and 1.74 μm emissions) that the optimal shift is 7 nm; this shift has been applied to the VIRTIS spectra present in this paper.

The 1.31 μm images have been included in order to show that the contrast between bright and dark regions of the images increases with wavelength: the contrast is roughly 2:1 for 1.31 μm images, 3:1 for 1.51 μm images, and 10:1 for 1.74 μm images. The radiation at all these wavelengths originates in the atmosphere below the clouds and is attenuated as it passes upwards through the cloud layer to space. Therefore, bright regions in all the images represent areas of low cloudiness, while dark regions represent thick cloud. The radiance at all three wavelengths is attenuated by the same clouds, so the images at the

three wavelengths show broadly the same contrast patterns. However, the contrast increases with wavelength, due to increasing extinction by the H_2SO_4 cloud particles (this is due both to an increase in the scattering cross-section and to a decrease in their albedo with increasing wavelength).

The relative intensities of the radiance at these three wavelengths are sensitive to the properties of the cloud particles [see e.g. Carlson et al 1993]. The three images (at 1.31, 1.51, and 1.74 μm) in the top panel of Fig. 3 look similar to each other, implying that there is little variation in cloud properties in this region (low- to mid-latitudes). On the other hand, the lower panels of Fig. 3, which show the polar region, show that the shorter-wavelength radiation is relatively less attenuated at very high latitudes than is the 1.74 μm radiance. This is consistent with relative ratios of 1.74 and 2.30 μm radiances observed in polar regions, which may indicate anomalously large particles in the polar vortex. [Wilson et al, 2008]. Thus, the absolute magnitude of the 1.51 and 1.55 μm emissions could be used to constrain cloud properties, however, we have not yet performed such an analysis due to the marginal signal to noise ratio at these wavelengths in the VIRTIS observations.

Observed spectra for the 1.48 – 1.58 μm region are shown in the right-hand panel of Figure 2. The two solid black lines in this figure represent an averaged spectrum for 'bright' and 'dark' populations of pixels, defined as the brightest 10% and darkest 10% of pixels in the 1.74 μm image. No limb-darkening correction was applied, but only pixels which have an emission angle less than 50° are considered. The dotted line at the bottom of the image represents the noise level of the data; it can be seen that these averaged spectra show a signal-to-noise ratio of 4-5.

Also plotted in the right hand panel of Fig. 2 is a synthetic spectrum as shown in the left hand panel, but degraded to VIRTIS-M spectral resolution. We note that, although the spectral bins in the –M channel are spaced every 9.5 nm, the spectral width is estimated to be 17 nm (This is the spectral width at 1.74 μm deduced by Bézard et al., 2009). Thus, the high-resolution spectrum shown in Fig. 2 has been convolved with a spectral ITF (instrument transfer function), which has been assumed to be a Gaussian shape with a FWHM of 17 nm. It can be seen that the radiative transfer model qualitatively reproduces the observed

spectrum. There is a discrepancy between the modelled and observed spectra of a few nm in the peak wavelengths of these two windows, which may be due to incomplete CO_2 absorption data; however, the relative magnitudes of the two peaks are well-reproduced by the model.

Conclusions

We have analysed newly-discovered thermal emission from the deep atmosphere of Venus at wavelengths of 1.51 and 1.55 μm, using the VIRTIS spectrometer on board Venus Express. With the low spectral resolution of VIRTIS-M, and the low signal-to-noise ratio available for this window, we are unable to constrain the properties of the lower atmosphere on the basis of the present data. However, the relative insensitivity of these windows to water or other trace gases in the deep atmosphere make them potentially useful for studying cloud properties, especially using a future instrument with increased signal-to-noise ratios and a higher spectral resolution.

Acknowledgments

We acknowledge the entire Venus Express and VIRTIS teams, as well as funding from national agencies STFC, ASI, CNES and NASA.

References

Allen, D. A., Crawford, J.W., 1984. Cloud structure on the dark side of Venus. Nature 307, 222–224.

Baines, K. H., Bellucci, G., Bibring, J.P., Brown, R.H., Buratti, B.J., Bussolletti, E., Capaccioni, F., Cerroni, P., Clark, R.N., Coradini, A., Cruikshank, D.P., Drossart, P., Formisano, V., Jaumann, R., Langevin, Y., Matson, D.L., McCord, T.B., Mennella, V., Nelson, R.M., Nicholson, P.D., Sicardy, B., Sotin, C., Hansen, G.B., Aiello, J.J., Amici, S., 2000. Detection of Sub-Micron Radiation from the Surface of Venus by Cassini/VIMS, Icarus 148 , 307-311, doi:10.1006/icar.2000.6519.

Bézard, B., de Bergh, C., Crisp, D., Maillard, J. P., 1990. The deep atmosphere of Venus revealed by high-resolution night-side spectra. Nature 345, 508–511.

Bézard, B., Tsang, C.C.C., Carlson, R.W., Piccioni, G., Marcq, E., Drossart, P., 2009, The Water Vapor Abundance Near the Surface of Venus from Venus Express / VIRTIS Observations, Journal of Geophysical Research, under review.

Carlson, R. W., Baines, K.H., Encrenaz, T., Taylor, F.W., Drossart, P., Kamp, L.W., Pollack, J.B., Lellouch, E., Collard, A.D., Calcutt, S.B., Grinspoon, D.H., Weissman, P.R., Smythe, W.D., Ocampo, A.C., Danielson, G.E., Fanale, F.P., Johnson, T.V., Kieffer, H.H., Matson, D.L., McCord, T.B., Soderblom, L., 1991. Galileo infrared imaging spectroscopy measurements at Venus. Science 253, 1541–1548.

Carlson, R. W., L. W. Kamp, K. H. Baines, J. B. Pollack, D. H. Grinspoon, T. Encrenaz, P. Drossart and F. W. Taylor, 1993. Variations in Venus cloud particle properties : a new view of Venus's cloud morphology as observed by the Galileo Near-infrared Mapping Spectrometer. Planet. Space Sci., 41 (7), 477-485.

Crisp, D., Allen, D.A., Grinspoon, D.H., Pollack, J.B., 1991. The dark side of Venus: Near-infrared images and spectra from the Anglo-Australian observatory. Science 253, 1263–1266.

Drossart, P., Piccioni, G., Adriani, A., Angrilli, F., Arnold, G., Baines, K., Bellucci, G., Benkhoff, J., Bezard, B., Bibring, J.-P., Blanco, A., Blecka, M., Carlson, R., Coradini, A., Di Lellis, A., Encrenaz, T., Erard, S., Fonti, S., Formisano, V., Fouchet, T., Garcia, R., Haus, R., Helbert, J., Ignatiev, N., Irwin, P., Langevin, Y., Lebonnois, S., Lopez-Valverde, M., Luz, D., Marinangeli, L., Orofino, V., Rodin, A., Roos-Serote, M., Saggin, B., Sanchez- Lavega, A., Stam, D., Taylor, F., Titov, D., Visconti, G., Zambelli, M., Hueso, R., Tsang, C., Wilson, C. and Afanasenko, T. Z., 2007. Scientific goals for the observation of Venus by VIRTIS on ESA/Venus Express mission. Planetary and Space Science 55, 1653-1672.

Erard, S., Drossart, P. Piccioni, G., 2009. Multivariate analysis of Virtis/Venus-Express night-side and limb observations, JGR-Planets, 114, E00B27, doi:10.1029/2008JE003116.

Hashimoto, G.L., Sugita, S. 2003. On observing the compositional variability of the surface of Venus using nightside near-infrared thermal radiation, Journal of Geophysical Research 108 (E9), 5109, doi:10.1029/2003JE002082.

Irwin, P.G.J., Teanby, N.A., de Kok, R., Fletcher, L.N., Howett, C.J.A., Tsang, C.C.C., Wilson, C.F., Calcutt, S.B., Nixon, C.A., Parrish, P., 2008. The NEMESIS planetary atmosphere radiative transfer and retrieval tool, Journal of Quantitative Spectroscopy and Radiative Transfer, 109 (6), p. 1136-1150, doi:10.1016/j.jqsrt.2007.11.006.

Kamp, L.W., Taylor, F.W., Calcutt, S.B., 1988. Structure of Venus's atmosphere from modelling of night-side infrared spectra. Nature 336, 360–362.

Lecacheux, J., Drossart, P., Laques, P., Deladerrière, F., Colas, F., 1993. Detection of the surface of Venus at 1.0 μm from ground-based observations, Planet. Space. Sci. 41, 543–549.

Marcq, E., Bézard, B., Drossart, P., Piccioni, G., 2008. A latitudinal survey of CO, OCS, H_2O and SO_2 in the lower atmosphere of Venus: spectroscopic studies using VIRTIS-H, J. Geophys. Res., doi:10.1029/2008JE003074, in press.

Piccioni et al., 2008. "The VIRTIS instrument on Venus Express", ESA-SP-1291. In press.

Pollack, J.B., Dalton, J.B., Grinspoon, D., Wattson, R.B., Freedman, R., Crisp, D., Allen, D.A., Bézard, B., deBergh, C., Giver, L.P., Ma, Q., Tipping, R., 1993. Near-infrared light from Venus's nightside: A spectroscopic analysis. Icarus 103, 1–42.

Rothman, L.S., and 30 colleagues, 2003. The HITRAN molecular spectroscopic database: edition of 2000 including updates through 2001, Journal of Quantitative Spectroscopy and Radiative Transfer. 82, 5–44. doi:10.1016/S0022-4073(03)00146-8

Seiff, A., Schofield, J., Kliore, A., Taylor, F., Limaye, S., Revercomb, H., Sromovsky, L., Kerzhanovich, V., Moroz, V. and Marov, M., 1985. Models of the Structure of the Atmosphere of Venus from the Surface to 100 Kilometers Altitude, Advances in Space Research 5(11), 3–58.

Taylor, F., D. Crisp and B. Bézard, (1997), Near-infrared sounding of the lower atmosphere of Venus, in *Venus II*, University of Arizona Press, 325–351.

Tonkov, M., Filippov, N., Bertsev, V., Bouanich, J., Nguyen, V.-T., Brodbeck, C., Hartmann, J., Boulet, C. and Thibault, F., 1996. Measurements and empirical modeling of pure CO_2 absorption in the 2.3μm region at room temperature: far wings, allowed and collision induced bands, Applied Optics 35(24), 4863–4870.

Tsang, C.C.C., Irwin, P.G.J., Taylor, F.W., Wilson, C.F., 2008. A Correlated-k Model of the Venus Nightside Near-Infrared Window Emissions from 1.0 to 2.5 μm, for the Retrieval of Minor Species from Venus Express/VIRTIS, Journal of Quantitative Spectroscopy and Radiative Transfer 109 (6), p. 1118-1135, doi:10.1016/j.jqsrt.2007.12.008.

FIGURE CAPTIONS

Fig. 1 – Synthetic spectrum of the nightside of Venus, at a spectral resolution of (thin line) 1 nm and (thick line) 10 nm. The near-horizontal lines across the middle of the image indicate the noise-equivalent signal radiance (NESR) for VIRTIS (Drossart et al., PSS 2007) with integration times of 1 second (dotted line) and 18 seconds (solid line).

Fig. 2: left panel: The solid line shows a synthetic spectrum, at 1nm spectral resolution, for water vapour abundances of (solid line) 30 ppm and (dot-dashed line) 100 ppm. The radiance scale is normalised to the peak radiance of the 30 ppm spectrum. The lower panel shows the location and relative strengths of water vapour absorption lines. The centre panel shows the contribution functions of the radiance at 1.51 μm with respect to temperature (solid line) and water vapour abundance (dashed line). Note that the spectrum has been convolved to 10nm spectral resolution before this function has been evaluated.
The right panel shows observed spectra from VIRTIS, observation VI0319_01. Two curves show average spectra over bright regions and dark regions of the image, as described in the text; the spectra have also been corrected for scattered sunlight, and a constant background level subtracted. The standard deviation of the measurements is indicated as a thick grey line at the bottom of the plot. The thick grey line shows the modelled spectrum of Fig. 2, convolved with a 17nm FWHM filter to simulate the spectral resolution of VIRTIS-M.

Fig. 3: panels show data from two observations (VI0319_00 in the top row and VI0373_00 in the bottom row), showing images at (left) 1.31 μm, (centre) 1.51 μm, and (right) 1.74 μm. The images show near-polar view of different regions of the Southern hemisphere; the observation shown in the top row covers latitudes from the equator (in the upper left hand corner) to -72°, while the observation in the lower row shows latitudes from -36° to the pole (at the bottom centre of image).

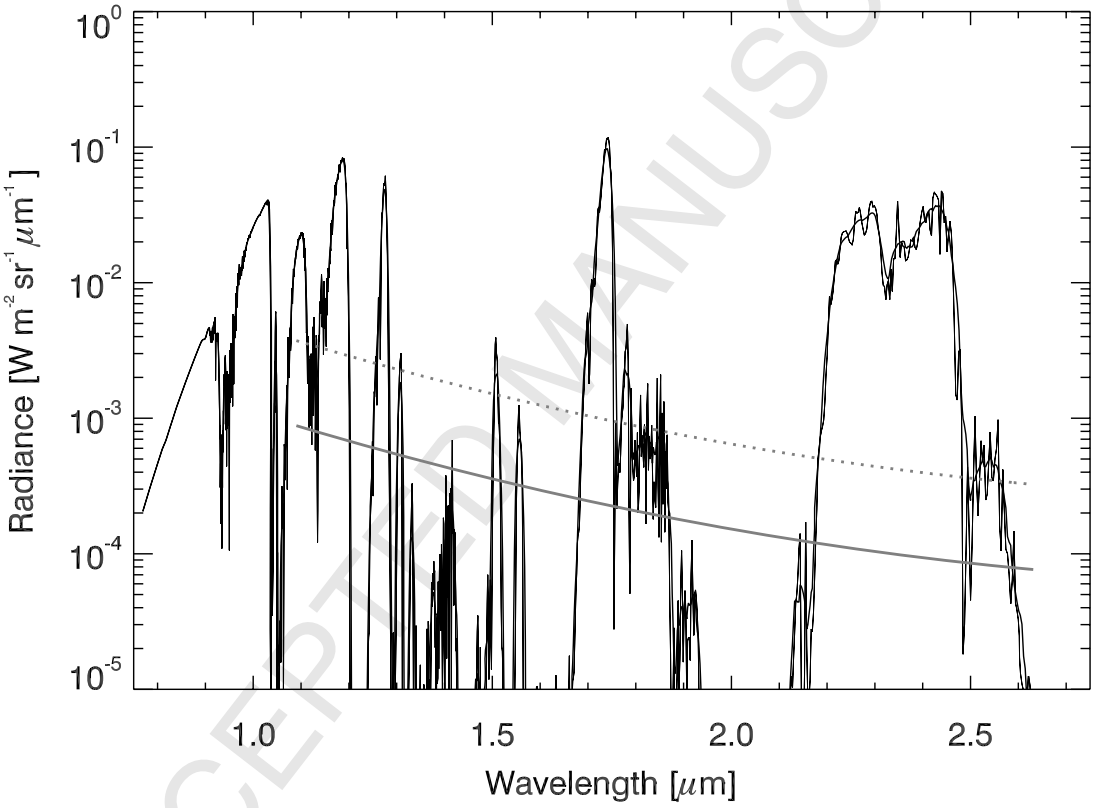

fullspectrum_revised

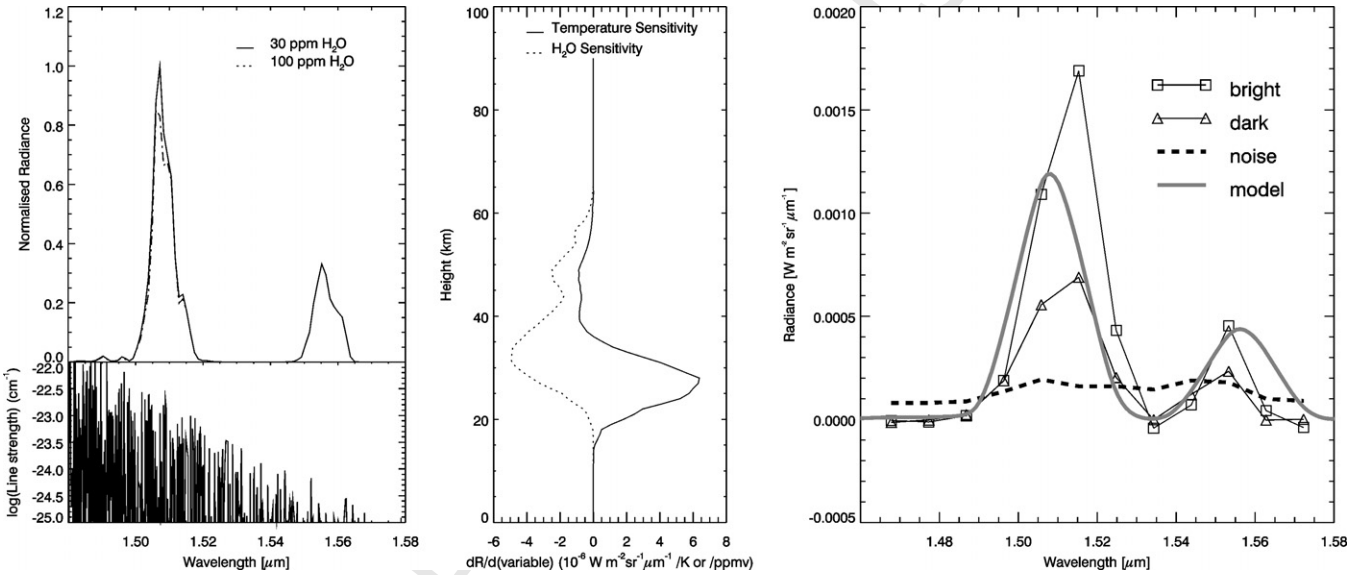

plot_rt4

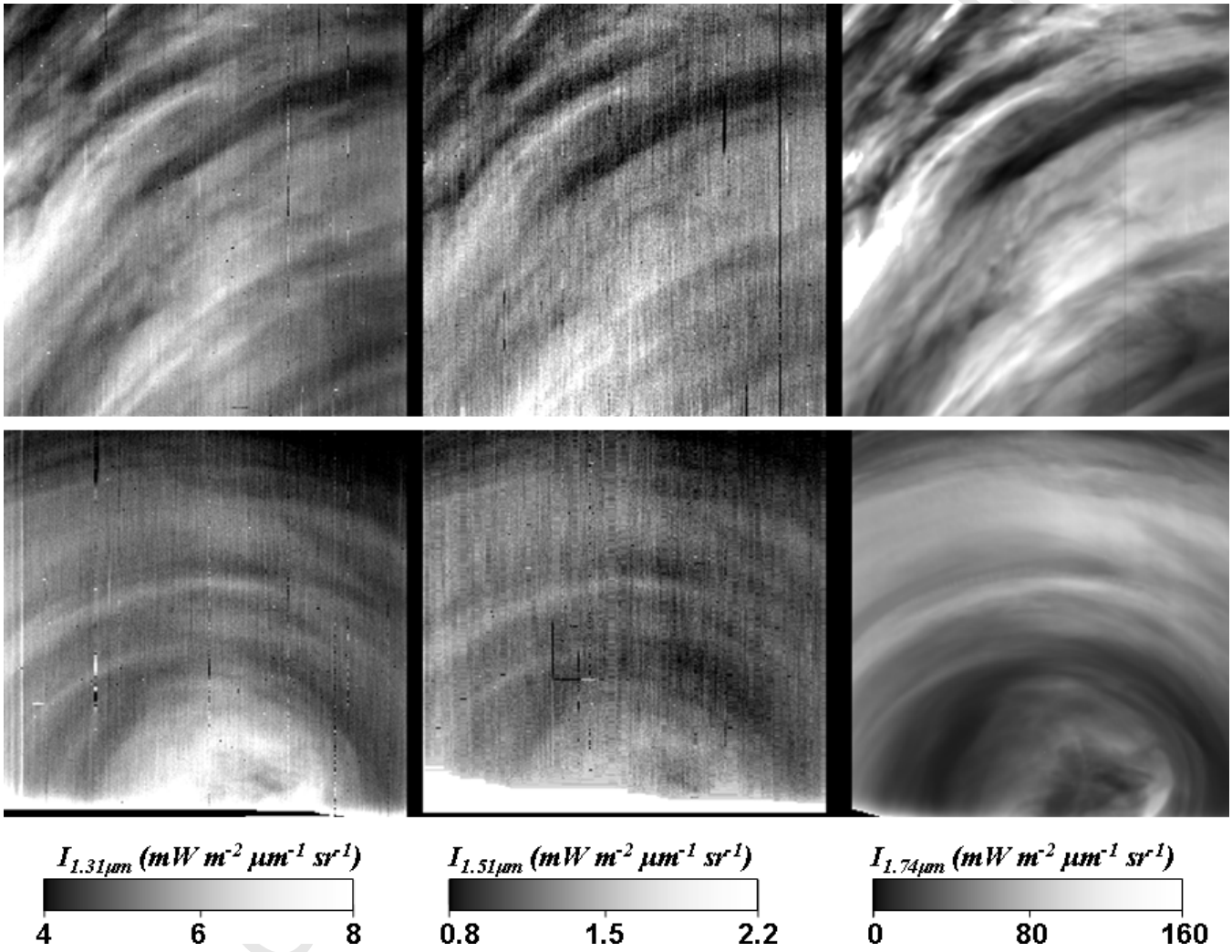

1.3um_image_figure_3_revised